A&A manuscript no.
(will be inserted by hand later)

Your thesaurus codes are:
11.01.2;11.09.1;11.17.2;11.19.1

ASTRONOMY AND ASTROPHYSICS
July 23, 1998

Kinematics of the Narrow-Line Region of NGC 1068 ⋆

M. Dietrich and S.J. Wagner

Landessternwarte Heidelberg, Königstuhl, D-69117 Heidelberg, Germany,

7 May 1998; accepted date

Abstract. We investigated the kinematics of the Narrow Line Region of NGC 1068. In order to study the kinematics and to determine whether the unusual broad line width can be attributed to motion of NLR clouds in a deep gravitational potential or to expanding shocks, we carried out spatially resolved echelle spectroscopy. High spectral resolution enables the identification of individual clouds in long slit spectra even if their angular separation is much smaller than the seeing limited resolution of ground-based instruments.
Most of the [OIII] line emission can be attributed to 12 clouds with an average angular separation of about 0.″3. These clouds differ in peak velocity by up to 2000 km s^{-1}, spanning the whole range of the integrated line profile with FWHM = 1150 km s^{-1}. The clouds do not delineate a simple rotational velocity field. We find evidence for shocks due to the interaction of the radio jet with the ambient NLR gas. The clouds which are attributed to shocks have a width of 350 km s^{-1} to 600 km s^{-1} while clouds with FWHM $\simeq$ 200 km s^{-1} seem to follow a circular velocity field. Therefore, the line width of individual clouds are an essential contribution to the integrated line width of the NLR of NGC 1068 which is not due only to gravitational forces but shocks playing an important role.

Key words: Galaxies: active, Seyfert — quasars: emission lines — galaxies: individual (NGC 1068)

1. Introduction

During the last years there is growing evidence that the structure and kinematics of the narrow-line region (NLR) of active galactic nuclei is complex and that it is not possible to describe the dynamics and the state of the line emitting gas with a uniform velocity field or a single excitation mechanism (e.g. Alloin et al. 1983; Whittle 1985; Viegas-Aldrovandi & Contini 1989; Cecil et al. 1990; Asif et al. 1997). Intensive HST studies of the NLR revealed an irregular morphology which is built up from several individual emitting complexes (cf. Evans et al. 1991; Macchetto et al. 1994; Capetti et al. 1995a; Weymann et al. 1997). Furthermore, it has been found that the morphology of the NLR in the optical is directly related to the radio emission (e.g. Capetti et al. 1997a; Gallimore et al. 1996a). Seyfert galaxies with a lobe-like radio structure (e.g. Mkn 78, Mkn 573) have bow-shock shaped emission line regions while a jet-like radio morphology (e.g. Mkn 3, Mkn 348) is related to a jet-like emission line structure (Capetti et al. 1996). This close correspondance between the optical and radio emission can be explained within the framework of the interaction of the radio jet with the NLR gas (cf. Taylor et al. 1992, Steffen et al. 1997).
A fundamental assumption in many models of the line-emitting AGN has been the idea that the width of emission lines reflects the strength of the gravitational potential at the luminosity-weighted radius where the corresponding line is emitted. Non-gravitational forces are not assumed to contribute to the line-widths of the NLR or broad-line region (BLR). This is independent of the details of the velocity field (chaotic or random motion) but contrasts with those models which in addition take into account radial motions or the influence of shocks as a significant contribution to the line shape.
The classical Seyfert 2 galaxy NGC 1068 is one of the best studied and nearest active galaxies. Therefore, it is a prime target to study the kinematics and the physical state of the line emitting gas of the NLR with spectroscopy at high spectral resolution. However, the line width (FWHM $\simeq$ 1150 km s^{-1}) is unusually large for a Seyfert 2 galaxy. We will assume a systematic velocity of v_{sys} = 1145 km s^{-1} for NGC 1068 (Allen et al. 1971) implying a distance of ∼23 Mpc (0.″1 corresponds to 11 pc, H_o=50 km s^{-1} Mpc^{-1}). This velocity is within the uncertainties identical with those given by Huchra et al. (1983) or Tully (1988).
It is known for more than 25 years that the NLR of NGC 1068 is clumpy due to several line emitting cloud complexes (Walker 1968; Anderson 1971). But the detailed structure of the NLR remained unresolved. Recent high resolution imaging studies using the HST have demonstrated that the NLR of NGC 1068 is composed of a large set of discrete cloud complexes with angular separation much smaller than the limited resolution of ground-based telescopes (e.g. Macchetto et al. 1994; Capetti et al. 1995a). The close correspondance of the radio morphology and of the NLR emission, already investigated by Wil-

Send offprint requests to: M. Dietrich, mdietric@lsw.uni-heidelberg.de

⋆ Based on observations collected at the European Southern Observatory, La Silla, Chile

son & Ulvestad (1983), has been studied in detail by Capetti et al. (1997b) making use of the high spatial resolution of the HST. They found evidence for the interaction of the central radio jet with the NLR gas which is consistent with the ionization properties of the line emitting gas.
In the following we will describe the observations of the 2 D-spectrograms which we observed (Sect. 2) and the method to achieve sub-arcsec resolution based on these spectra (Sect. 3). In Sect. 4 we will present the results of the deconvolution of the highly structured [OIII] 5007 emission line profile. These results will be compared with recent HST studies and will be discussed in the context of the radio-jet NLR gas interacting model of NGC 1068 (Axon et al. 1998).

2. Observations and Reduction

Generally, it is difficult to obtain information about the spatial structure of the NLR using ground-based telescopes due to seeing limitation. However, the nearest Seyfert galaxies provide the possibility to study the spatially resolved NLR. But even for these AGNs sub-arcsec resolution is necessary to investigate distinct emitting knots of the NLR. Using long-slit spectroscopy with high spectral resolution ($\sim$15 km s^{-1}) it is possible to achieve a spatial resolution which is significantly smaller than $1''$.
We observed the central region of NGC 1068 on Dec. 21st and Dec. 22nd, 1993 using the CASPEC spectrograph in the short camera mode at the 3.6m telescope of the European Southern Observatory (ESO), La Silla, Chile. The 2 D spectra were obtained with a Tektronix 512 x 512 CCD. The pixel size of 27 μm corresponds to $0.''71$ perpendicular to the dispersion axis. The 2 D spectrograms cover a wavelength range of 4737 Å—6220 Å. The slit width was set to $1.''5$ projected onto the sky. The slit length was limited to $6''$ to avoid an overlap of adjacent echelle orders and to determine the contribution of the scattered light. Echelle spectrograms were obtained for two different position angles, PA=32° and PA=122°, i.e. parallel and perpendicular with respect to the major axis of NGC 1068 (e.g. Wilson & Ulvestad 1983). For each position angle three exposures with an integration time of 50 minutes each were recorded. The three spectrograms per position had a slightly different spatial registration. This helped to overcome the disadvantage of slight spatial undersampling along the slit. ThAr spectra were taken for each spectra for wavelength calibration and internal flat field exposures after each object exposure to minimize the influence of the ordershift of the consecutive observations. Spectra of the standard stars HR 718 and HR 3454 were observed each night for flux calibration. Our spectra of NGC 1068 do not contain point sources since none of the clouds was found to be unresolved in the HST data (Macchetto et al. 1994). This prohibits the exact determination of the spatial point spread function in our 2 D spectrograms which is due to seeing and residual guiding errors during each exposure. The seeing was measured for several stars observed during the night and yields $1.''7$ (Dec. 21) and $1.''3$ (Dec. 22).
The standard echelle reduction including subtraction of bias and scattered light, flat-field correction, wavelength calibration, and rectification of the 2 D spectrograms was carried out using standard routines of the MIDAS and IRAF echelle reduction packages. The wavelength calibration of the ThAr frames yielded a stepsize of 0.131 Å px^{-1} in the blue increasing to 0.172 Å px^{-1} in the red part of the spectrograms with an uncertainty of 0.013 Å. The spectra were rebinned to a uniform wavelength scale of 0.131 Å px^{-1}. The spectral resolution of the spectra was measured using night sky lines of [OI] 5577 and NaD 5893/96. The FWHM amounts to (0.283±0.004) Å corresponding to 15.2 km s^{-1}. The absolut wavelength calibration shows an uncertainty of 0.03 Å i.e. less than 2 km s^{-1}. A sensitivity function was computed for each order. It was assumed that this function is constant in spatial direction. The uncertainty introduced by the echelle order overlap is less than 6 %. Finally, the spectra of the different echelle orders were merged yielding a continuous spectrum for the spectral range given above. The spectral range of the [OIII] 5007 line is displayed in Fig. 1. It is clearly visible that the emission line profile shows significant spatial variations in strength and structure on scales less than $1''$. The uncertainty of the line profile shape has been investigated using the [OIII] 5007 line profile of the individual spectra. In Fig. 2 the differences as well as the ratio of the line profile with each other are shown. It can be seen that the uncertainty of the profile shape is less than 5%. Only the first spectrum taken at PA=32° introduces a small feature in the ratio. It is caused by an enhenced flux in the region at

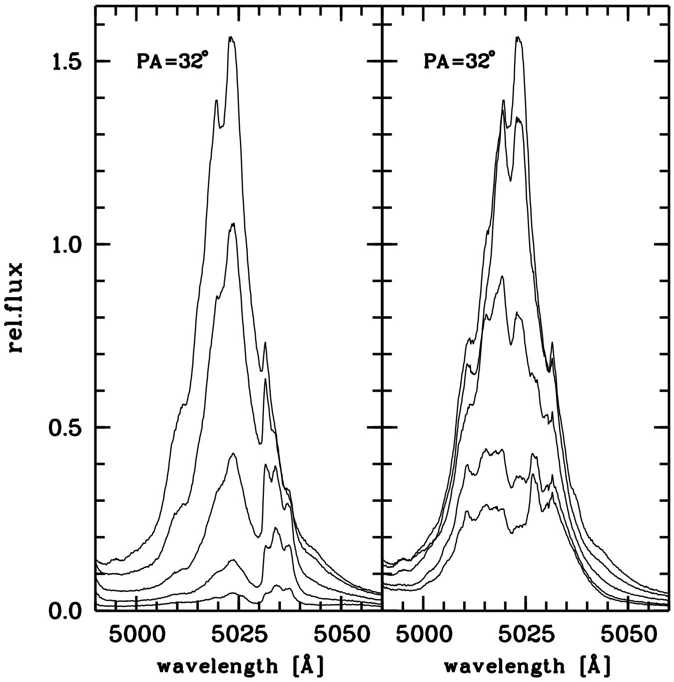

Fig. 1. The spatial variation of the [OIII] 5007 emission line of NGC 1068 (PA=32°). The left panel shows the spectra starting in the south-west up to the maximum of the light distribution. The right part of the figure displays the variations from the center up to the north-east region of the 2 D echelle spectrogram. The spectra are separated in space by $0.''71$.

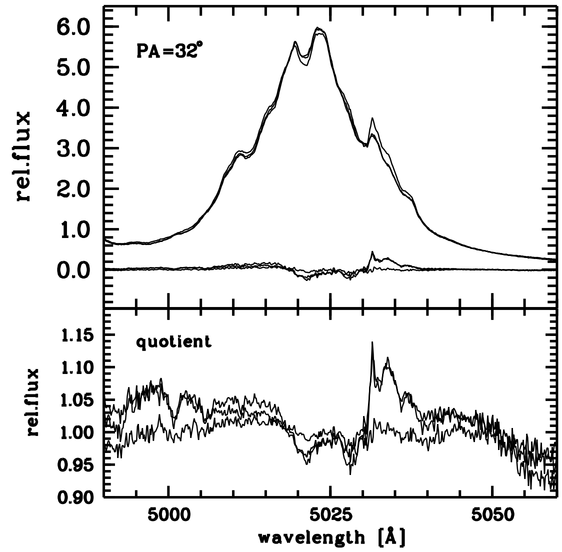

Fig. 2. Comparison of the emission line profile of [OIII] 5007 obtained for PA=32° (upper panel). The differences of the three individual spectra are shown at the bottom of the upper panel. The ratios of the spectra are displayed in the lower panel. The deviation is of the order of less than 5 %. Only a spike at $\lambda \simeq 5035$ Å due to the first spectrum taken at this position angle introduces a greater uncertainty.

$\lambda \simeq 5033$ Å located 1.″5 southwest from the center in spectrum 1. It might be due to an cosmic ray event since the profile match of spectrum 2 and 3 for PA = 32° is better than 2% (Fig. 2).

3. Analysis of Echelle Spectrograms

3.1. The Method of sub-arcsec Mapping

For more than 25 years it is known that the NLR of NGC 1068 consists of at least four distinct emission complexes (Walker 1968; Glaspey et al. 1976; Alloin et al. 1983) which seem to be related to the elongated radio structure (Wilson & Ulvestad 1983). High spectral resolution spectroscopy provided indications of several individual clouds by deconvolving the structured but spatially not resolved emission line profiles with gaussian components. Recent observations of the NLR with high spatial resolution show that it is highly structured on scales of less than 0.″1 e.g. NGC 1068 (Evans et al. 1991; Macchetto et al. 1994), NGC 4151 (e.g. Pelat & Alloin 1982; Weymann et al. 1997). The individual emission knots can be used as probes to map the velocity field of the NLR. Furthermore, the physical state of the gas (temperature, density, elemental abundance) can be investigated as well as the excitation mechanisms, i.e. photoionization by the central continuum source or shock heating due to interaction of the radio jet with the NLR gas.
The drawback of seeing limited ground-based observations can be overcome using spatially resolved longslit spectroscopy with high spectral resolution. For a single slit position the identification of individual emission line regions can be still ambiguous for some components. This degeneration will be solved if at least two different slit orientations are recorded.
In Fig. 3 the method is displayed for an ensemble of seven discrete emission line knots. Each knot has been assigned an internal velocity distribution (60 km s^{-1}, 240 km s^{-1}), an arbitrary radial velocity, and a spatial extension and location. The spatial width was set arbitraly to 0.″1, 0.″3, and 0.″5, respectively. The separation of the clouds is of the order of 0.″7. This cloud ensemble was convolved with a gaussian point spread function to simulate seeing of 0.″75. If this apparently featureless, asymmetric structure is observed in longslit mode, 2 D spectrograms will be obtained which are shown in the right panel of the top row and in the panel of the bottom row (Fig. 3). In each case no definite identification can be found for two features based on the information of a single l-v map. But this problem will be subdued if the information of at least two slit orientations is taken into account. Making use of both measurements the location of the seven emission line regions can be reconstructed using the x-v and y-v information provided by the 2 D spectrograms (Fig. 3).

3.2. Decomposition of the [OIII] 5007 line profile

HST imaging observations of NGC 1068 showed that the [OIII] emission is due to a large number of individual clouds with angular separations which are too small to permit direct decomposition in seeing limited data (e.g. Macchetto et al. 1994). The luminosity distribution of the individual clouds clearly illustrates that at least a dozen of these clouds contribute about 80% of the total emission.
In the following we concentrate on the emission of [OIII] 5007, a strong, unblended line which is generally assumed to be representative for the narrow-line emission from an AGN. The total line flux cannot be due to one or two cloud complexes only since the integrated line width is larger than 1100 km s^{-1} (Fig. 1). The finite number of clouds which are major contributors to the total [OIII] emission are spread over a wavelength range covering nearly 2500 km s^{-1}. The position of each of these clouds in the l-v space has been determined following the the method described in Sect. 3.1.
Because we are interested in the emission line profiles we corrected for the underlying stellar continuum. A linear continuum fit was calculated. The fit of the continuum flux was determined by the mean of a 10 Å wide window centered at 4785 Å and 5100 Å, respectively. The linear fit was subtracted from the spectra. Next, the spectra were transformed into the velocity space assuming $v_{sys} = (1145 \pm 25)$ km s^{-1} (Allen et al. 1971) as radial velocity of NGC 1068. The spectra of [OIII] 5007 were combined to a space-velocity-map (l-v-map) covering -1600 km s^{-1} to $+1200$ km s^{-1} in velocity space and $-3.''0$ to $+3.''0$ in spatial direction for both position angles. Finally, the echelle spectra were rebinned to a uniform spatial stepsize of 0.″143 px^{-1} (Fig. 4).
These l-v-maps have been reconstructed to identify individual emission line complexes within the NLR of NGC 1068. We assumed that the components can be represented by 2 D gaussian curves, i.e. the width in veleocity space of the individual com-

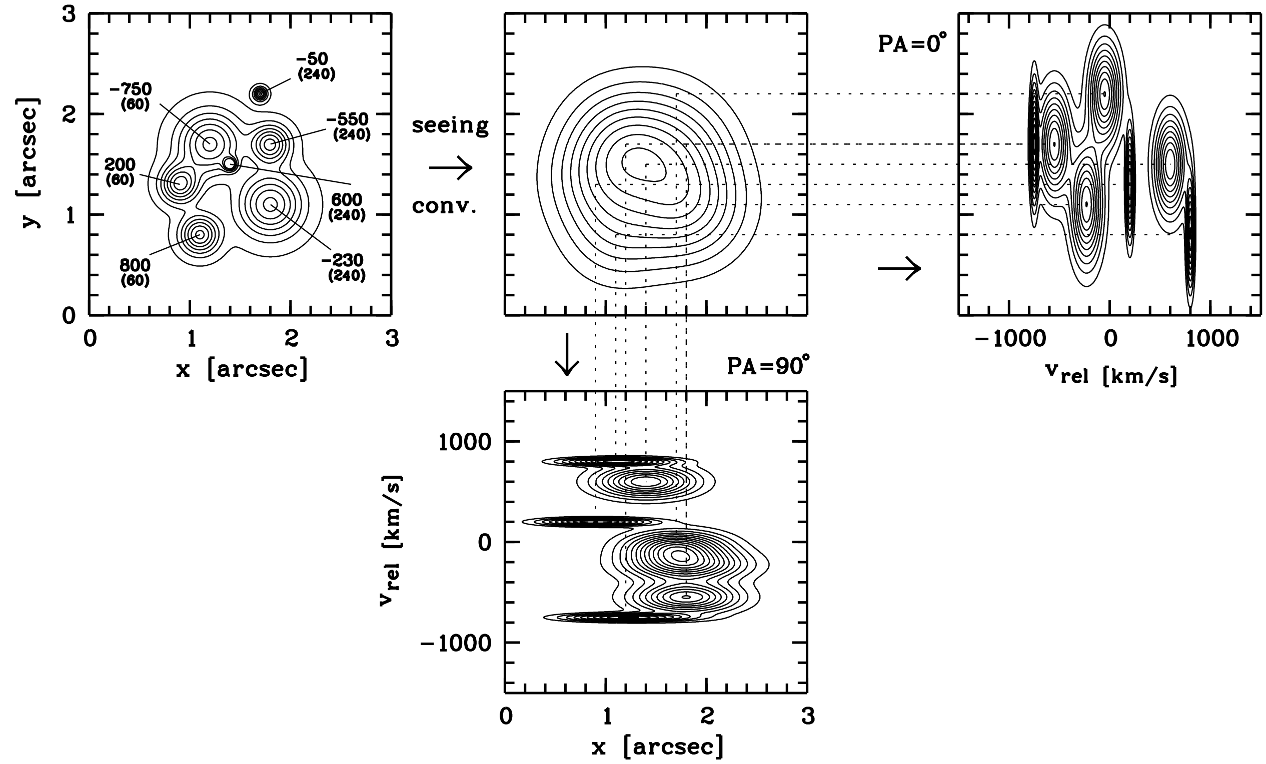

Fig. 3. An ensemble of seven cloud complexes is shown in the top left panel. The assigned radial velocity and the FWHM of the velocity dispersion of the individual clouds are given as labels in the top left panel. The velocity dispersion amounts to 60 $\mathrm{km\,s^{-1}}$ and 240 $\mathrm{km\,s^{-1}}$. The middle panel of the upper row displays the ensemble after it has been convolved with a gaussian point spread function (FWHM = 0.″75). Observing this structure with longslit spectroscopy at slit orientations of PA = 0° and PA = 90° the discrete clouds will be separated in velocity space.

ponents is dominated by random turbulent motion within the cloud complex. The FWHM should be less than 300 $\mathrm{km\,s^{-1}}$. The FWHM in spatial direction was restricted to 1.5 times of the seeing. By inspection of the profiles in spatial and velocity direction we started to remove the components in order of decreasing strength to minimize the residuum. Since this approach yields no unique solution we have tested several combinations of very broad and narrow profiles in the reconstruction procedure. But the components given in Table 1 seem to provide the most reasonable solution within the restrictions we put on the individual components. The location of the fitted gaussian components in velocity space given by the three exposures of each position angle is constant within $\sim$ 10 $\mathrm{km\,s^{-1}}$. The uncertainty of the location perpendicular to the dispersion axis is of the order of 0.″1. Some components cannot be distinguished using only the 2 D spectrogram of PA = 32°. Due to the orientation of the slit the central 1.″5 x 1.″5 have been observed twice. Therefore, ambiguities for the central components can be solved. The fitting parameters in velocity and FWHM are consistant (Table 1). With only 16 components it is possible to describe the intensity distribution of the emission in the [OIII] 5007 line profile. The residuals of the [OIII] 5007 l-v-maps are of the order of $\approx$ 12% of the total intensity of the [OIII] 5007 emission-line flux.

Table 1. Mean fitting parameter of the gaussian components used for the reconstruction of the [OIII] 5007 emission line profile for a position angle of PA=32° and PA=122°. The identification of the components given by Evans et al. (1991) is presented in column ident.

comp	v [$\mathrm{km\,s^{-1}}$]		FWHM [$\mathrm{km\,s^{-1}}$]		ident.
	32°	122°	32°	122°	
1	−138± 3	−130± 9	298±18	291±24	D
2	−413±10	−420± 5	298±13	287±18	F
3	+207±21	+210± 7	632±24	577±12	C
4	−818±25	−855±13	682±31	585± 7	B
5	+937± 6	+937± 6	561±27	550±13	E
6	−730±12	—	432±13	—	G
7	−1013±16	—	338±24	—	
8	+113± 3	—	283±17	—	
9	+360±17	—	153±24	—	
10	+503± 6	—	177±12	—	
11	+690±12	—	161±14	—	
12	+360±12	—	690±27	—	
13	−653±25	—	706±15	—	
14	+368± 3	—	361±14	—	
15	−650± 5	−642± 3	181± 6	165±15	
16	−412±31	−385± 5	165±12	157±14	

4. Results and Discussion

The central part of NGC 1068 covered by the slit configuration we used is shown together with our CASPEC echelle spectro-

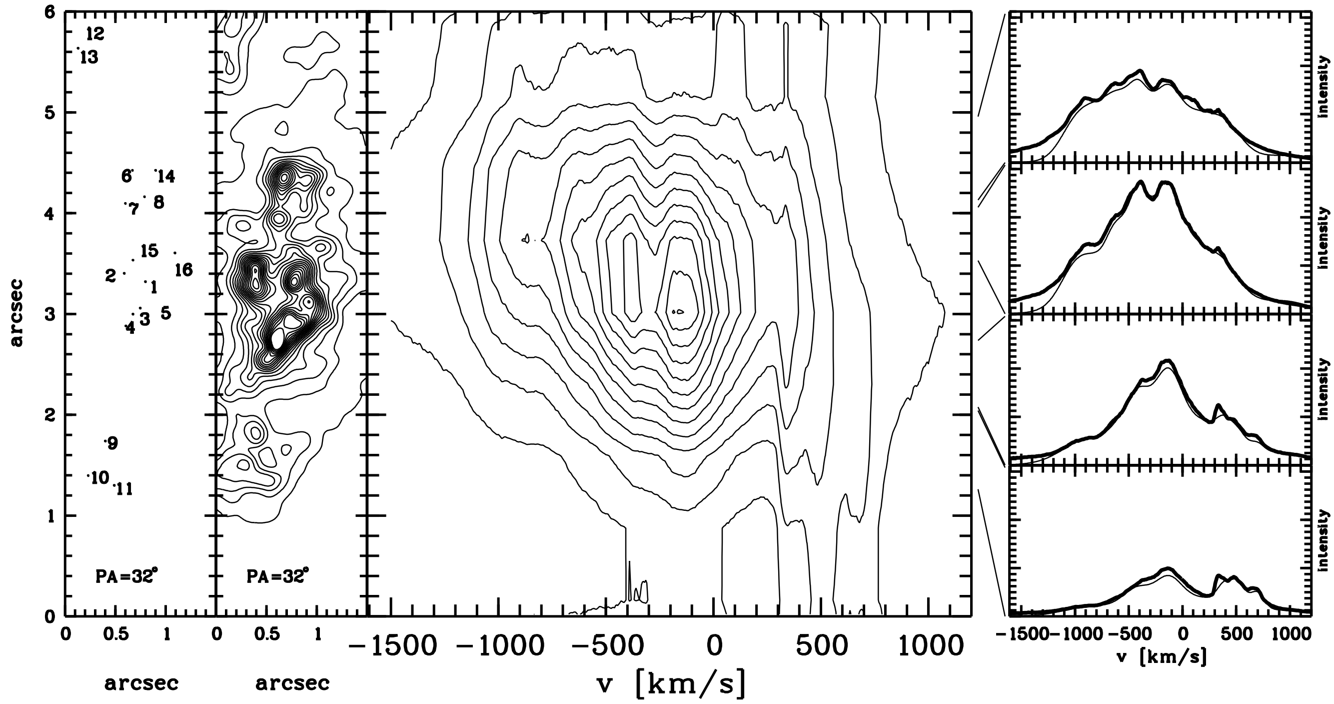

Fig. 4. The numbers in the first panel at the left side of the figure show the position of the components given in Table 1 which have been derived from the decomposition process of the [OIII] 5007 profile. In the following panel the inner region of NGC 1068 is displayed which we observed. This HST-image taken with the F501N filter (Macchetto et al. 1994) has been convolved with a 0.″1 gaussian filter. The l-v-map of the [OIII] 5007 emission line is displayed at the right part of the slit-view of the central region. The four panels at the right side show a comparison between the observed line profiles for several spatial locations (thick line) with the line profiles which were recovered by the reconstruction of the l-v-map (thin line).

gram observations in the same spatial scaling in Fig. 4. The l-v-map of the [OIII] 5007 emission line profile is clearly structured on scales of less than 1.″0 and the extension in velocity space amounts to $\approx$ 2500 km s^{-1} (Fig. 1 and Fig. 4). The dominant feature is a double peaked structure located at the center with v $\simeq$ -250 km s^{-1} and an emission triplett at v $\simeq$ 500 km s^{-1} in the southwest direction. A comparison between the observation and the reconstruction model is shown for representative parts of the l-v map in the Fig. 4 (right four panels). Even in the outer parts of the l-v map of the [OIII] 5007 emission line profile the model fit is close to the observed intensity distribution.

The results of the reconstruction of the [OIII] 5007 emission line, i.e. the spatial location of individual emission complexes have been compared with HST-observations obtained by Macchetto et al. (1994). The HST image shown in Fig. 4 was taken with the F501N narrow-band filter corresponding to [OIII] 5007. It was smoothed with a gaussian filter of FWHM = 0.″1 to emphasize the dominant [OIII] 5007 emission features. Six bright emission line knots are visible in the smoothed HST image and at least 10 weaker structures. In the original NGC 1068 HST-frame more than 30 cloud complexes can be identified.

Due to the orientation of the slit the central 1.″5 have been observed twice while the components located in the SW and NE are covered only for PA=32°. The location of components showing ambiguities in this regions of the l-v map have been determinated using the intensity ratio. For the central part both slit orientations have been used to recover the location of the components in spatial coordinates. The analysis of the l-v intensity distribution have been perfomed independently for the individual 2 D spectrograms. The fitting parameters of the gaussian curves which we have derived to reconstruct the l-v-maps of the [OIII] 5007 emission line are given in Table 1.

We measured the relative distance of the cloud complexes with respect to cloud 1, i.e. cloud D following the nomenclature of Evans et al. (1991). The location of the clouds parallel to the major axis were derived from 2 D spectrograms with PA = 32° and the location perpendicular to the major axis were provided by 2 D spectrograms obtained at PA = 122°. For component 1 – 5, i.e. B – F (Evans et al. 1991) and component 15 and 16 we compared the positions calculated from our 2 D spectrograms with the measured positions of the high resolution HST image of the central region of NGC 1068. The mean deviation amounts to 0.″02±0.″11. The identification of component 9, 10, and 11 in the southwest direction of the nucleus can be taken as reasonable as well as the identification of 6, 7, 8, and 14 northwest from the nucleus which based on the intensity ratios. The mean deviation taking these components in addition into account yields 0.″03 ± 0.″11. Therefore, the components given in Table 1 can be identified within ≈0.″1 with the discrete emission line knots visible in the HST image.

The relative velocities of the fitted gaussian components range from $v \simeq -1000\,\mathrm{km\,s^{-1}}$ to $v \simeq +950\,\mathrm{km\,s^{-1}}$. The uncertainty of the position in the velocity-space which has been estimated from the independent reconstruction of the individual echelle spectra is of the order of $\Delta v = (11 \pm 8)\,\mathrm{km\,s^{-1}}$. Shifts of this order produce already characteristic sharp spike-like features in the l-v-maps. The location of those components in velocity space which have been observed for both position angles are nearly identical within $\sim 15\,\mathrm{km\,s^{-1}}$ (Table 1). Most of the components have a velocity dispersion of the order of 300 $\mathrm{km\,s^{-1}}$ or even less given by the FWHM of the fitted gaussian curve (Table 1). The structures with a FWHM $\simeq$ 600 $\mathrm{km\,s^{-1}}$ can be ascribed more complex regions which might consist of at least two individual emission line complexes. Especially the components 3, 4, 5, 12, and 13 provide evidence for a complex substructure or high internal motions regarding their extension in velocity space of FWHM = $(623 \pm 63)\,\mathrm{km\,s^{-1}}$.

The l-v-map of the observed central region of the NLR of NGC 1068 provide evidence for a complex velocity field structure (Fig. 5). The emission line components in the southwest (9, 10, 11) show velocities in a range of +300 $\mathrm{km\,s^{-1}}$ to +700 $\mathrm{km\,s^{-1}}$ while the emission line regions in the northeast show a wide spread of velocities ranging from +500 $\mathrm{km\,s^{-1}}$ to −1000 $\mathrm{km\,s^{-1}}$ (6 - 8 and 12 - 16). Studies with lower spectral resolution provide some evidence for an emission line complex in the southwest with $v \simeq 400$ $\mathrm{km\,s^{-1}}$ and FWHM $\simeq$ 400 $\mathrm{km\,s^{-1}}$ (Pecontal et al. 1997). These structure has been resolved into the components 9 - 11 based on the 2 D echelle spectra we have taken.

Capetti et al. (1995b, 1997a) have determinated the position

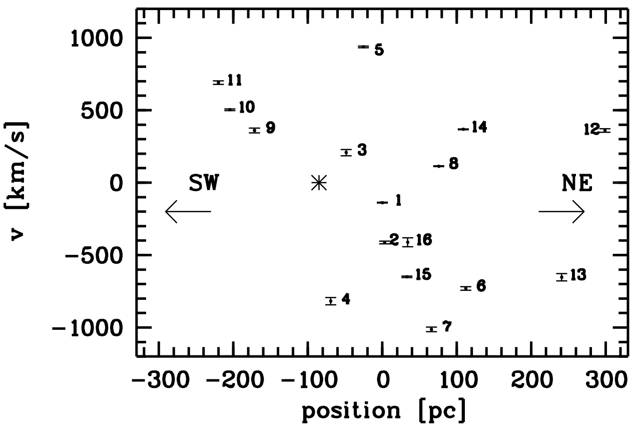

Fig. 5. The location of the components which have been used to deconvolve the [OIII] 5007 line profile in a rotation curve for PA = 32°. The asterisk indicates the location of the nucleus.

of the nucleus of NGC 1068 using HST polarimetry measurements of the NLR. The derived position of the nucleus can not be associated with cloud B, i.e. component 4 or with the center of the twin crescent structure described by Macchetto et al. (1994). The derived location of the nucleus indicates that the radio emission structure now appears to be more closely associated with the emission morphology of the NLR than previuosly. If the nucleus is assigned the systematic velocity of NGC 1068 it can be added to the rotation curve plot displayed in Fig. 5. It is plotted as an asterix.

For some of the emission-line regions spectra were taken with HST (P.I. Ford). The spectra corresponding component 1 and 2 were recorded at Jun, 6th 1991, spectra of component 6 and 9, 10, 11 were recorded with the HST on March, 1st 1993. An HST spectrum of component 3 were observed on Jun, 25th 1991 and of component 4 on October, 29th 1990. We have retrieved the spectra from the HST archive and transformed them into velocity space in the same way as the 2 D echelle spectrograms which we have observed. The shape of the line profiles have been compared. The profiles of these HST [OIII] 5007 emission line spectra are consistent with the shape and velocities which we have derived from our 2 D echelle spectrograms.

Recently the NLR of NGC 1068 has been observed with HST in the longslit spectroscopy mode (Axon et al. 1998). The results of our reconstruction of the [OIII] 5007 line has been compared with the spectrum they have obtained for POS 3 which corresponds spatially to component 6, 7, 8 of our study (Fig. 4). They found that at the jet axis the emission line split up into two velocity systems separated by $\approx$1500 $\mathrm{km\,s^{-1}}$. The region east of the jet axis shows $v \approx -1300$ $\mathrm{km\,s^{-1}}$ while at the west side $v \approx +150$ $\mathrm{km\,s^{-1}}$. The velocities we derived for component 6 and 7 are in good agreement with these measurements as well as for component 8 (see Table 1). A similar result has been obtained by Pecontal et al. (1997) who found −800 $\mathrm{km\,s^{-1}}$ for cloud G. Furthermore, the radial velocity we detected for component 16 is nearly identical with the radial velocity provide by Axon et al. (1998). Axon et al. explained the large velocity split which we also found in the region of cloud G (component 6, 7, 8) as the result of the interaction of the radio jet with the NLR gas in terms of an expanding and cooling cocoon around the jet (cf. Taylor et al. 1992; Steffen et al. 1997). The interaction of the radio jet with the NLR has been already mentioned by Wilson & Ulvestad (1983) who found hints for a velocity split in the NE region of $\approx$1100 $\mathrm{km\,s^{-1}}$.

In addition to the cloud G complex there is another region in the NLR showing a strong velocity split in the line profile. The features 3, 4, 5 (B, C, E following the nomenclature of Evans et al. 1991) show a steep gradient ($\sim 30\,\mathrm{km\,s^{-1}\,pc^{-1}}$) of increasing velocity in north-south direction (Fig. 5, Table 1). The velocity split between component 3 and 4 amounts to $\approx$ 1000 $\mathrm{km\,s^{-1}}$. A similar velocity split was found by several authors (e.g. Wilson & Ulvestad 1983; Cecil et al. 1990). Meaburn & Pedlar (1986) derived from their echelle spectra of the central NLR evidence for two components with $v_1 \simeq -760$ $\mathrm{km\,s^{-1}}$ (FWHM$_1 \simeq 870$ $\mathrm{km\,s^{-1}}$) and $v_2 \simeq +340$ $\mathrm{km\,s^{-1}}$ (FWHM$_2 \simeq 640$ $\mathrm{km\,s^{-1}}$). These measurements correspond well with component 3 and 4 of our investigation. We associated component 3 and 4 with the twin crescent structure mentioned by Macchetto et al. (1994). The kinematical behaviour of these components is a further indication that the nature of these cloud complexes is different from the regular NLR gas. The polarisation of this structure amounts to

$\sim 100\,\%$ in the ultraviolet after correction for dilution (Capetti et al. 1995a). Therefore, it might be a reflection image of the obscured central region of NGC 1068. Due to the large velocity split it might be possible that this structure also indicates interaction of the radio jet with the NLR gas. The importance of the influence of the radio jet to the emission line gas of the NLR has been shown based on the close correspondance of the morphology even at smaller scales (e.g. Gallimore et al. 1996a,b; Steffen et al. 1997). In the radio domain is has been shown that this structure is located close to the point where the orientation of the radio jet axis changes from PA $= 11^\circ$ to PA $= 33^\circ$. Since the change of the orientation of the jet axis can be expected for an interaction of the jet with a cloud these structure is suggested to be also explained within a shock model, too (Gallimore et al. 1996b).
The components 1, 2, 9, 10, 11, 15, 16 seem to follow a regular rotation with regard to the location of the nucleus of NGC 1068 (Fig. 5).
Some evidence for the distinction of the different components regarding their kinematics and even their possible excitation mechanism is provided regarding the velocity dispersion of the line emitting gas. These results suggest a picture of the NLR of NGC 1068 where shocks introduced by the radio jet - NLR gas interaction play an important role. The components 6, 7, 8, 14 which can be associated with the shock proposed by Axon et al. (1998) show a FWHM $= (350\pm60)$ km s^{-1}. The emission line complexes corresponding to component 3, 4, 5 can be characterized with FWHM $\simeq (600\pm50)$ km s^{-1}. Finally, structures whose kinematics seem to be dominated by gravitational forces show smaller velocity dispersions of FWHM $\simeq (210\pm65)$ km s^{-1}. Component 1 and 2 (i.e. D and F) show a complex morphology and might consist of more individual cloud systems. The value of the velocity dispersion is reduced to FWHM $= (165\pm10)$ km s^{-1} taking into account only component 9, 10, 11, 15, 16.
Since the highly structured [OIII] 5007 line profile can be reconstructed with a small number of components with FWHM less than 600 km s^{-1} it seems not necessary to ascribe the large profile width of [OIII] to a single blue shifted broad component of FWHM $\simeq 1700$ km s^{-1} (Pelat & Alloin 1980). Furthermore, Cecil et al. (1990) provide evidence from Fabry-Perot interferometry study of the inner region of NGC 1068 that the profile of the [NII] emission lines is better described with individual components in the blue and red wing than with a single broad component.
Comparison with several studies of the inner region of NGC 1068 provide evidence for the identification of the components we derived from the reconstruction of the [OIII] 5007 line profile. The physical state of the NLR gas and the excitation mechanisms will be studied making use of the red part of the spectrum of NGC 1068 which we already obtained as 2 D spectrogram.

5. Conclusions

We have observed 2 D echelle spectrograms of the central region of NGC 1068 take advantage of the spectral and spatial resolution. This data provide a tool to resolve the structure and the velocity field of the NLR on scales which are smaller than the seeing limited resolution. Emission line complexes which differ significantly in velocity can be distinguished on subarcsec scales. The space-velocity-maps of strong, unblended emission lines in NGC 1068 are structured on scales less than $1.''0$. We have shown that the [OIII] 5007 emission line can be reconstructed with 16 components only assuming a simple gaussian profile to represent the discrete emission line complexes. The derived velocities of the components range from -1000 km s^{-1} to $+1000$ km s^{-1}.
Comparison with HST-studies and the radio morphology of the NLR suggests that two larger structures consisting of several components which are characterized by strong velocity splits of the order of 1000 km s^{-1} can be associated with expanding and cooling cocoons around the radio jet. These shocks can be explained in the interaction scenario of the radio jet with the ambient NLR gas (e.g. Taylor et al. 1992; Steffen et al. 1997). The FWHM of these components is significantly larger than 300 km s^{-1}. The cloud complexes which can be associated with the twin crescent structure (Macchetto et al. 1994) show a FWHM $\simeq (600\pm50)$ km s^{-1}. The components which show an internal velocity dispersion of $\approx$200 km s^{-1} or even less seem to follow a regular circular motion.
The reconstruction of the [OIII] 5007 emission line profile provides evidence for several kinematical subsystems and the important role of the interaction of the radio jet with the NLR gas which causes regions of shock heated gas.

References

Allen R.J., Darchy B.F., Lauqué R., 1971, A&A 10, 198
Alloin D., Pelat D., Boksenberg A., Sargent W.L.W., 1983, ApJ 275, 493
Anderson K.S., 1971, ApJ 162, 743
Asif M.W., Unger S.W., Pedlar A., et al., 1997, MNRAS 284, L15
Axon D.J., Marconi A., Capetti A., et al., 1998, ApJ 496, L75
Capetti A., Axon D.J., Macchetto F.D., Sparks W.B., Boksenberg A., 1995a, ApJ 446, 155
Capetti A., Macchetto F.D., Axon D.J., Sparks W.B., Boksenberg A., 1995b, ApJ 452, L87
Capetti A., Axon D.J., Macchetto F.D., Sparks W.B., Boksenberg A., 1996, ApJ 469, 554
Capetti A., Macchetto F.D., Lattanzi M.G., 1997a, ApJ 476, L67
Capetti A., Axon D.J., Macchetto F.D., 1997b, ApJ 487, 560
Cecil G., Bland J., Tully R.B., 1990, ApJ 355, 70
Evans I.N., Ford H.C., Kinney A.L., et al., 1991, ApJ 369, L27
Gallimore J.F., Baum S.A., O'Dea C.P., Pedlar A., 1996a, ApJ 458, 136
Gallimore J.F., Baum S.A., O'Dea C.P., 1996b, ApJ 464, 198

Glaspey J.W., Walker G.A.H., Stockton A., 1976, ApJ 210, 27
Huchra J., Davis M., Latham D., Tonry J., 1983, ApJS 52, 89
Macchetto F.D., Capetti A., Sparks W.B., Axon D.J., Boksenberg A., 1994, ApJ 435, L15
Meaburn J., Pedlar A., 1986, A&A 159, 336
Pecontal P., Ferruit P., Binette L., Wilson A.S., 1997, in Proc. of the NGC 1068 Ringberg Workshop 1996, eds. J.F. Gallimore and L.J. Tacconi, p.168
Pelat D., Alloin D., 1980, A&A 81, 172
Pelat D., Alloin D., 1982, A&A 105, 335
Steffen W., Gomez J.L., Raga A.C., Williams R.J.R., 1997 ApJ 491, L73
Taylor D., Dyson J.E., Axon D.J., 1992, MNRAS 255, 351
Tully R.B., 1988, Nearby Galaxy Catalog, Cambridge University Press
Viegas-Aldrovandi S.M., Contini M., 1989, ApJ 339, 689
Walker M.F., 1968, ApJ 151, 71
Weymann R.J., Morris S.L., Gray M.E., Hutchings J.B., 1997, ApJ 483, 717
Whittle M., 1985, MNRAS 213, 33
Wilson A.S., Ulvestad J.S., 1983, ApJ 275, 8

Acknowledgements. The investigators have benefited from support from Deutsche Forschungsgemeinschaft grant SFB 328 . We are grateful to Dr. A. Jüttner who carried out most of the observations.